Genomic analysis of diffuse intrinsic pontine gliomas identifies three molecular subgroups and recurrent activating ACVR1 mutations

Jason Fangusaro, *Emory University*
Pawel Buczkowicz, *University of Toronto*
Christine Hoeman, *Duke University*
Patricia Rakopoulos, *Hospital for Sick Children*
Sanja Pajovic, *Hospital for Sick Children*
Louis Letourneau, *McGill University*
Misko Dzamba, *University of Toronto*
Andrew Morrison, *Hosp Sick Children*
Peter Lewis, *Rockefeller University*
Eric Bouffet, *Hospital for Sick Children*

Only first 10 authors above; see publication for full author list.

Copyright information:

Genomic analysis of diffuse intrinsic pontine gliomas identifies three molecular subgroups and recurrent activating *ACVR1* mutations

A full list of authors and affiliations appears at the end of the article.

Abstract

Diffuse Intrinsic Pontine Glioma (DIPG) is a fatal brain cancer that arises in the brainstem of children with no effective treatment and near 100% fatality. The failure of most therapies can be attributed to the delicate location of these tumors and choosing therapies based on assumptions that DIPGs are molecularly similar to adult disease. Recent studies have unraveled the unique genetic make-up of this brain cancer with nearly 80% harboring a K27M-H3.3 or K27M-H3.1 mutation. However, DIPGs are still thought of as one disease with limited understanding of the genetic drivers of these tumors. To understand what drives DIPGs we integrated whole-genome-sequencing with methylation, expression and copy-number profiling, discovering that DIPGs are three molecularly distinct subgroups (H3-K27M, Silent, MYCN) and uncovering a novel recurrent activating mutation in the activin receptor *ACVR1,* in 20% of DIPGs. Mutations in *ACVR1* were constitutively activating, leading to SMAD phosphorylation and increased expression of downstream activin signaling targets ID1 and ID2. Our results highlight distinct molecular subgroups and novel therapeutic targets for this incurable pediatric cancer.

Keywords

DIPG; H3F3A; K27M-H3.3; ALT; ACVR1; MYCN; ID2; PDGFRA

Dr. Cynthia Hawkins, MD, PhD, FRCPC, Division of Pathology, The Hospital for Sick Children, 555 University Avenue, Toronto, ON, M5G 1X8, Phone: (1) 416-813-5938, Fax: (1) 416-813-5974, cynthia.hawkins@sickkids.ca. Dr. Oren Becher, MD, Departments of Pediatrics and Pathology, Preston Robert Tisch Brain Tumor Center, Duke University Medical Center, Phone: (1) 919-681-0172, oren.becher@duke.edu.
*equally contributed to the manuscript
#co-corresponding, co-senior authors

Brain tumors are the largest group of solid tumors and the leading cause of cancer-related deaths in childhood[1]. The most devastating of these is DIPG, which is almost universally fatal[2,3]. Despite collaborative efforts to improve treatments, survival has remained static over decades, and DIPGs are now the main cause of brain tumor death in children. Diagnosis of DIPG is based on a combination of clinical and radiologic findings; a tissue biopsy is rarely acquired. Radiation is the mainstay of therapy but offers only symptom control and so far chemotherapy has shown no benefit[4]. A potential contributor to the failure of DIPG clinical trials is the use of agents targeting the genetic alterations of adult glioblastomas (GBMs)[5]. A number of recent studies have reported differences at both the copy number and expression level that distinguish pediatric DIPG from both their adult and pediatric supratentorial GBM counterparts[6–9], indicating that they may be separate biologic entities requiring their own therapeutic strategies. Recent identification of frequent histone 3 mutations (K27M-H3) in DIPG has suggested that both genetic and epigenetic mechanisms may be important drivers of these tumors[10–12]. However, the complete genetic and epigenetic landscape of DIPG and the functional role that histone modifications may play in DIPG remain unknown. This data is critical for the development of better therapies for these children.

We integrated deep-sequencing analysis of 36 tumor–normal pairs (20 whole genome sequencing (WGS; Illumina Hiseq 2000) and 16 whole exome sequencing (WES; Applied Biosystems SOLiD 5500xl)), with comprehensive methylation (28 DIPGs; Illumina Infinium450K methylation array), copy number (45 DIPGs, Affymetrix SNP6.0) and expression data (35 DIPGs; Illumina HT-12 v4) (Supplementary Table 1). All coding somatic single nucleotide variants (SNVs) identified in the combined cohort are listed in Supplementary Table 2 including novel mutations in *ACVR1*. We did not find mutations in *BRAF* or *IDH1* or structural rearrangements in *FGFR1* or *MYB* in our DIPG cohort. Verification of somatic alterations was conducted on all 35 pairs using Fluidigm Array Ion Torrent chip sequencing (Supplementary Table 3). Further, for key SNVs, a validation cohort of an additional 25 tumors was also tested. This analysis reveals, in contrast to what was previously considered to be one disease, DIPG represents three distinct subgroups with different methylation, expression, copy number alteration (CNA) and mutational profiles.

Unsupervised subgrouping of DIPG patients based on CpG island methylation (see Methods section) resulted in three distinct subgroups; MYCN, Silent, and H3-K27M (Fig. 1a). This subgrouping was supported by multiple analyses including principal components analysis (Fig. 1b), non-negative matrix factorization (Fig. 1c) and consensus clustering (Fig. 1d). Subgroup-specific differences were supported by integration of mutation, structural, expression and clinical data (Fig. 2). The identification of DIPG subgroups will have important implications for design of appropriate therapy for these tumors.

The MYCN subgroup has no recurrent mutations but is instead characterized by hypermethylation, high grade histology, and chromothripsis on chromosome 2p leading to recurrent high level amplification of *MYCN* and *ID2* (Table 1, Supplementary Fig. 1 – 3). It over-expresses *MYCN* 4-fold and 8-fold and *ID2* 2.5-fold and 5-fold vs. the H3-K27M and Silent groups, respectively. The top most over-expressed genes in the MYCN group include *FAP*, *HRSP12*, and *DYX2*. Therapies aimed at targeting altered histone modifications will not be effective in this subgroup. Rather these children will potentially benefit from

therapies targeting MYCN or possibly ID2. The Silent subgroup has silent genomes based on both WGS structural and SNP6.0 copy number analysis and has a lower mutation rate than the other two subgroups (median of 0.11 mutations per Mb (range 0.02–0.19) in the silent cohort vs. 0.99 mutations per Mb (range 0.19–24) in the other two groups, p = 0.05 (Supplementary Table 4)). All DIPGs with low-grade astrocytoma (LGA) histology are from this group, although interestingly there is no difference in overall survival in comparison with the other subgroups. These patients were diagnosed at a significantly younger age (4.81 ± 1.64 years for Silent group patients vs. 6.89 ± 2.62 years for non-Silent group patients; p = 0.04). K27M-H3 is present in 44% (K27M-H3.3 at 33% and K27M-H3.1 at 11%) but there are no recurrent copy number changes as observed in the MYCN and H3-K27M subgroups. At the expression level, the Silent subgroup shows over-expression of WNT pathway genes (Supplementary Table 5), as well as *MDM2, MSMP* and *ADAM33* compared with the other two subgroups (Table 1). Importantly, neither the MYCN nor the Silent subgroup DIPGs have receptor tyrosine kinase amplification suggesting this group of inhibitors will be less effective in these patients.

H3-K27M subgroup DIPGs are highly mutated in either H3.3 (*H3F3A)* or H3.1 (*HIST1H3B* and *HIST1H3C*). This group has highly unstable genomes (Segmentation Analysis of SNP6 data; 497 CNA per genome vs. 300 CNA per genome in the Silent group; p = 0.04). Alternative lengthening of telomeres (ALT via Telomere Restriction Fragment assay[13], C-circles[14] and/or telomere length from WGS) is exclusively associated with the H3-K27M subgroup; only two of these harbor *ATRX* mutations. ALT positive patients are significantly older at the time of diagnosis (Supplementary Fig. 4, p < 0.001). Similarly, *PVT-1/MYC* and *PDGFRA* gains/amplifications (Fig. 2a) and structural variants (Supplementary Fig. 5) are exclusive to this group. *TP53* mutations are enriched in this group (67.9% vs. other groups 33.3%, p = 0.007). Given the complexity and heterogeneity of H3-K27M subgroup genetics, if therapies targeting the histone mutations become available, this subgroup will likely require multi-modal therapies.

Certain mutations and structural variants are significantly more likely to co-occur - specifically K27M-H3.3 with *PDGFRA* amplifications (OR = 8.0, p = 0.0127), and K27M-H3.1 with *ACVR1* mutations (OR = 15.8, p = 0.0004) (Fig. 2b). Conversely, *MYCN* amplifications are statistically less likely to occur if a K27M-H3 mutation is present (OR = 0.019, p = 0.0103; Fig. 2b). Patients carrying K27M-H3.3 mutations are more likely to have GBM histology (OR = 5.3 p = 0.0035), while K27M-H3.1 mutations are more likely to occur in patients with anaplastic astrocytoma histology (OR = 7.1, p = 0.016) and in younger patients (K27M-H3.1: 4.11 ± 2.03 years vs. WT-H3.1: 6.50 ± 3.50 year; p = 0.040) (Fig. 2c). *TP53* mutations are more likely to occur in patients with GBM histology regardless of K27M-mutational status (OR = 8.3, p = 0.0039) and unlikely to occur in patients with LGA histology (OR = 0.046, p = 0.0040) (Fig. 2c). A summary of molecular and clinical features observed among MYCN, Silent and H3-K27M DIPG patients is found in Table 1.

After *H3F3A* and *TP53*, the next most frequently mutated gene in DIPG is *ACVR1* (activin A receptor, type I), a novel cancer gene. Mutations of *ACVR1* in four DIPGs (c.617G>A) result in a R206H (Fig. 3a) substitution. One DIPG had a mutation of a neighboring codon (Q207E). Two DIPGs had a c.983G>A (G328E) mutation and five DIPGs in our cohort had

a c983G>T mutation which results in a G328V (Fig. 3a) substitution. In total 20% of DIPG have *ACVR1* mutations. *ACVR1* encodes for the Activin A (ALK-2) receptor involved in BMP (bone-morphogenic protein) signaling[18]. The R206H substitution is in the GS (glycine-serine rich) domain, and is the most common mutation responsible for an autosomal dominant disease of the connective tissue, fibrodysplasia ossificans progressiva (FOP), in which endothelial cells are sensitized to bone morphogenic protein (BMP) signaling, transitioning to osteoblasts[18]. The G328E and Q207E mutations are described as rare mutations in FOP patients[19,20]. The G328V substitution has not been previously reported in FOP patients or in cancer. Mutations on the G328 residue occur in the kinase domain and are spatially near the GS-domain[20] and similarly to the R206H substitution, are thought to weaken the GS-domain resulting in a ligand-independent, constitutively active receptor. Phospho-SMAD1/5 was increased in DIPG patients with *ACVR1* mutations as compared to ACVR1-WT patients (Fig. 3b).

To determine the biological consequence of *AVCR1* mutations *in vitro*, we transfected immortalized normal human astrocytes (iNHA) with 3x Flag tagged pCDH511b expression vectors containing either G328V-ACVR1 and/or K27M-H3.3. Western blot analysis showed endogenous expression of ACVR1 in all cells, with flag ACVR1 and higher total ACVR1 expression in transfected cells. To determine if the *ACVR1* mutant activates the BMP signaling pathway we tested for phospho-SMAD1/5 by Western blot. Only cells transfected with G328V-ACVR1 showed phospho-SMAD1/5 positivity (Fig. 3c). To test downstream pathway activation, we performed quantitative-PCR for ID1 and ID2, which are known targets of BMP signaling[15–17]. Expression of either K27M-H3.3 or G328V-ACVR1 alone led to a 2-fold increase in ID1 and ID2 expression, while co-expression of K27M-H3.3 and G328V-ACVR1 resulted in a nearly 4-fold increase in ID1 and ID2 expression, suggesting an additive effect (Fig. 3d). G328V-ACVR1 increased growth rate of iNHA as compared to empty vector controls ($p = 0.0034$, Fig. 3e). An increase in phospho-SMAD1/5 was also seen by Western blot in P3 murine brainstem progenitor cells from Nestin tv-a p53 floxed mice infected *in vitro* with RCAS R206H-ACVR1 or G328V-ACVR1 vs. WT-ACVR1 ($p<0.05$, data not shown). Brainstem progenitor cells infected with mutant *ACVR1* showed increased proliferation by BrdU incorporation ($p<0.05$, Fig. 3f).

To assess the impact of K27M-H3.3 on gene expression and methylation patterns as well as its potential transformative capacity, iNHA cells were transfected with N-terminally Flag tagged expression vectors containing WT-H3.3, K27M-H3.3 or empty vector (EV) control. Clones expressing comparable amounts of WT-H3.3 and K27M-H3.3 protein based on Western blot analysis (Supplementary Fig. 6a) and verified by immunofluorescence staining to localize to the nucleus (Supplementary Fig. 6b) were selected and pooled to remove clonal variations in phenotype. Compared to controls, K27M-H3.3 iNHA cells had a significantly reduced proliferation rate when grown adherently in DMEM (Supplementary Fig. 6c) and grew semi-adherently when seeded in neural stem cell media (NSC) (Supplementary Fig. 6e). Compared to adherent K27M-H3.3 iNHA, the semi-adherent K27M-H3.3 iNHA in NSC media had increased expression of SOX2 by immunofluorescence staining with no marked changes in GFAP, Nestin, TUJ1 or O4 (Supplementary Fig. 7). Alterations in both expression (Illumina HT-12v4) and methylation (Illumina Infinium450K) profiles of the K27M-H3.3 expressing cells vs. both WT and EV

controls was observed (Supplementary Fig. 6f). The top pathways perturbed by K27M-H3.3 expression corresponded to molecular and cellular functions especially an increase in cell-to-cell signaling (p = 0.00882, z-score 2.365) and a decrease in cell cycle progression (p < 0.00001, z-score -1.347). The top molecular and cellular functions affected by methylation changes in K27M-H3.3 mutated cells were embryonic development (p < 0.00001), decreased cell growth and proliferation (p = 0.00103), and increased cell-to-cell signaling (p < 0.00001). K27M-H3.3 cells did not form colonies in soft agar. K27M-H3.3 cells showed reduced global H3K27 trimethylation (H3K27me3) levels compared to controls (Supplementary Fig. 6d). Similarly, immunohistochemical staining of patient DIPGs showed a decrease in global H3K27me3 levels in K27M-H3.3 positive tumors compared to WT tumors (Supplementary Fig. 6g,h). Global levels of H3K27Ac, H3K4me3 and H3K9Ac were not altered in a mutation-dependent manner (data not shown).

Interestingly, K27M-H3.3 expression also leads to increased *ID1* and *ID2* expression yet does not induce pSMAD1/5 suggesting an alternate pathway. pSMAD1/5 expression was also only observed in DIPG patients with *ACVR1* mutations and not in K27M-H3 mutated but *ACVR1* wild-type DIPG. Our in vitro data suggest an additive effect of the combination of mutant *ACVR1* and *H3F3A* in increasing ID1 and ID2 levels. Further, a subset of DIPG patients with K27M-H3.3 mutations overexpress ID2, and MYCN subgroup patients have genomic amplification of *ID2* with corresponding increased expression suggesting a potential common ID2-related mechanism in DIPG tumorigenesis. ID2 may play a role in negatively regulating cell differentiation[21] and its expression has been associated with poor prognosis in other cancers[22–24]. Morphological changes, differential expression of stem cell markers, as well as global methylation and gene expression changes in iNHA following K27M-H3.3 expression suggests a cellular reprogramming event. However, further investigation into the effects of K27M-H3.3 and *ACVR1* mutations in DIPG tumorigenesis is warranted.

Our results highlight the many pathways to tumorigenesis in DIPG. This complexity needs to be considered when designing new therapeutic approaches in order to improve outcome for these children.

Online Methods

Patients and Samples

Biological material and clinical data was gathered for 74 DIPG samples, including normal brain and/or peripheral blood if available. DIPGs were diagnosed by a neuroradiologist based on MRI imaging. A contrasting lesion with diffuse involvement of at least 50% of the pons was required for DIPG diagnosis. All patient material was collected after receiving informed consent and was approved by the institutional review board of contributing centers. Twenty of these patients were pre-treatment samples (2 non-treated patients from autopsy), and 54 were post-treatment autopsy samples. The median age of diagnosis was 6.37 years with a median survival of 10.4 months.

Whole genome sequencing alignment and structural variants

The entire genomes of twenty DIPG tumor and matched normal DNA pairs were sequenced using next generation Illumina technologies. The DNA samples were paired-end-sequenced on an Illumina HiSeq2000) using DNA fragments 259-333bp in size with 100bp read length. The mean coverage was 35-67X for tumor and 28-74X for normal. BWA alignment tool was used to map all reads to GRCh37/hg19 using default parameters[25]. PCR duplicates were removed from alignments using PicardTools 1.77 (Supplementary Table 6). Structural variants (SV) were identified using PRISM 1.1.6 and PRISM CTX 1.0.1[26]. Recurrent SVs (Supplementary Table 7) were found after subtracting common SVs[27] and all SVs found in normal tissue and were visually validated using DNAC algorithm and SNP6.0 data in Partek Genomics Suite (v.6.6) as well as WGS data in Savant (v2.0.3)[28], and Integrated Genomics Viewer (v2.2). Prediction of structural variants in chromothriptic regions was performed by discordant read-pair clustering. Discordant read-pairs (fragment size $> 3 \cdot \sigma + \mu$) were initially selected for by greedy clustering using a sliding window of $15 \cdot \sigma$ and refined by clipped read mappings (Supplementary Fig. 8). Localization of chromothriptic event was predicted using Hidden-Markov-Model (HMM) informed by depth of coverage and discordant read-pairs. Maximum likelihood copy counts of chromothriptic regions was determined as previously described[29].

Exome capture was carried out with SOLiD (Applied Biosystems). Sequence data were aligned to the GRCh37/hg19 human reference genome assembly; duplicate and non-uniquely mapping reads were excluded. One hundred and fifty one sequence variants in 128 genes were validated using PCR amplification by Fluidigm arrays and ion torrent chips (Life Technologies). These SNVs were selected for validation based on variant allele frequency from WGS/WES and those found to be significantly altered upon analysis of the combined cohort with MutSig (Broad Institute), an algorithm testing whether the observed mutations in a gene are not simply a consequence of random background mutation processes (Supplementary Table 6).

Methylation Profiling

Comprehensive methylation profiling of 28 DIPG samples at the Microarray Centre (University Health Network, Toronto, ON) using the Illumina Infunium450K array (Illumina, San Diego, CA). Bisulphite conversion was carried out using the EZ DNA Methylation Kit (Zymo Research, Irvine CA) as per manufacturer's specifications. Methylation profiling iNHA transfected with K27M-H3.3 and WT-H3.3 vectors was also assessed on this array. DNA was extracted using the DNeasy kit (Qiagen, Mississauga, ON) according to the manufacturer's protocols. Subgrouping and clustering based on differential CpG probe methylation was performed and validated using multiple programs and algorithms including nonnegative matrix factorization (NMF) (GenePattern, Broad Institute), consensus hierarchical clustering (GenePattern; Broad Institute, ConsensusClusterPlus; Bioconductor/R and MultiExperiment Viewer, Dana-Farber Cancer Institute), Kmeans clustering (GenePattern; Broad Institute and ConsensusClusterPlus; Bioconductor/R), silhouette clustering (ConsensusClusterPlus; Bioconductor/R) and significance analysis of microarrays (SAM; MultiExperiment Viewer, Dana-Farber Cancer Institute). Subgroups were validated for significance by SigClust (Bioconductor/R).

Gene expression profiling

Expression profiling was conducted on 35 DIPG samples and 10 normal brain controls at the Microarray Centre (University Health Network, Toronto, ON) using the DASL protocol for Illumina HT-12 V4 BeadChip array (Illumina, San Diego, CA). Differential gene expression in NHA transfected with K27M-H3.3 and WT-H3.3 vectors was also assessed on this array. RNA was extracted using the QIAshdredder and RNeasy kit (Qiagen, Mississauga, ON) according to the manufacturer's specifications. Quality of the RNA was assessed using the Bioanalyzer 2100 (Agilent Technologies, Böblingen, Germany). RNA Integrity Number (RIN) ranged from 1.3 to 8.2. Microarray data was normalized in Partek Genomics Suite v6.6 (Partek Incorporated, St. Louis, MO) using per-probe median centered quantile normalization. Data analysis was conducted on Log_2 transformed data or fold-change data (vs. non-neoplastic brain). Genes differentially expressed among the subgroups were identified using one-way ANOVA and significance was corrected for false discovery rate.

Copy number analysis

Copy number analysis was conducted for 40 DIPG samples using SNP6.0 (Affymetrix, Santa Clara, CA). Digestion, labeling and hybridization of DNA were performed by The Centre for Applied Genomics at the Hospital for Sick Children or at the Microarray Centre at the University Health Network. CEL data was analyzed for copy number alterations using segmentation tool and hidden Markov model in Partek Genomics Suite (v6.6) (Partek Incorporated, St. Louis, MO) and Genotyping Console 4.1 (GTC4.1; Affymetix) as previously described[9].

In vitro modeling of K27M-H3.3 and G328V-ACVR1

Immortalized NHA cells (iNHA)[30] were grown in Dulbecco's modified eagle medium (DMEM) supplemented with 10% fetal bovine serum (FBS, Invitrogen). Cells were tested and found to be negative for mycoplasma. Cells were passaged at 80% confluence. Wild-type (WT-H3.3) and mutant (K27M-H3.3) *H3F3A* clones were created by site direction mutagenesis and PCR using pCMV SPORT6 (Adgene, Cambridge, MA) plasmid containing mouse H3F3A cDNA. Expression of flag tagged H3F3A WT and K27M was established by cloning corresponding cDNAs into p3xflagCMV10 (Sigma-Aldrich, Oakville, ON) vectors (see Supplementary Table 8 for primer sequences). Clones were confirmed by bidirectional Sanger sequencing. Cells were transfected by Fugene6 transfection reagent (Promega, Madison, WI) and according to the manufacturer's instructions.

To make stable transfectants, iNHA cells were co-transfected with a DNA fragment containing the hygromycin gene. Stably transfected clones were selected with 300μg/ml of hygromycin and pooled to eliminate clonal variations in phenotype. For the isolation of DNA and RNA used for expression and methylation arrays, respectively, cells were harvested at P4 and P15 at about 80% confluence. Total cell pellet for each sample was divided into 2 parts, one used for the isolation of genomic DNA and the other used for the isolation of RNA. Genomic DNA was isolated using the DNeasy blood and tissue kit (Qiagen, Mississauga, ON) followed by bisulfite conversion using EZ DNA Methylation Kit (Zymo research). Total RNA was isolated by RNeasy kit (Qiagen). iNHA from p4 and p15

were analyzed on methylation (Infinium 450K) and expression arrays (Illumina HT-12 v4) by the similar methods described for patients.

ACVR1 mutants were created from *ACVR1* cDNA using the QuikChange Site-Directed Mutagenesis Kit (Stratagene, Mississauga, ON) (see Supplementary Table 8 for primer sequences). Mutation was created at position c.983G>T resulting in amino acid change G328V. The G328-ACVR1 mutant was then sub-cloned into the pCDH511b (System Biosciences, Mountain View, CA), in frame with 3x FLAG tag at the 3′ end of the cDNA with pCDH511b, pCDH511b-G328V-ACVR1, pCDH511b-K27M-H3.3, or pCDH511b-G328V-ACVR1 and pCDH511b-K27M-H3.3. Cells were harvested 72 hours after transfection and protein and RNA was extracted for Western blot and Q-PCR analysis, respectively. Western blot was conducted using the following antibodies: pSMAD1/5 (1:1000, Cell Signaling, Danvers, MA), total SMAD1 (1:1000, Cell Signaling, Danversm MA), anti-FLAG (1:1000, Sigma, Oakville, ON) and ACVR1 (1:1000, Cell Signaling, Danvers, MA). Reverse transcriptase was conducted using RevertAid First Strand cDNA Synthesis Kit (Thermo Scientific, Ottawa, ON). See Supplementary Table 8 for real-time PCR primer pairs.

Cell counting and cell proliferation

Cell counting on K27M-H3.3 and G328V-ACVR1 as well as control iNHA cells was performed in triplicate using the automated Vi-Cell Viability Analyzer from Beckman-Coulter (Mississauga, ON). Cell proliferation was measured by bromodeoxyuridine (BrdU) incorporation. In brief, Np53fl murine brainstem progenitors were plated in a 96-well flat bottom plate (10×10^3 cells/well) in triplicate and incubated with ACVR1 WT, R206H, or G328V virus for 48 hours. Subsequently, cells were then pulsed with BrdU and treated according to the manufacturer's protocol. Absorbance was measured using a Molecular Devices Versa Max Tunable Microplate.

Immunohistochemistry

Available surgical and autopsy material was immunohistochemically stained with selected antibodies against H3K27me3, H3K27Ac, H3k4me3 and H3K9ac. Five micrometer sections of DIPG tissue-microarrays (TMA) constructed in our lab or tissue sections were cut from paraffin blocks and mounted on positively charged slides. The sections were baked overnight at 60°C. Wax was removed by several xylene washes followed by tissue hydration by immersion in decreasing concentrations of ethanol in distilled water. The tissue sections were heat treated in citrate buffer for the purpose of antigen retrieval. Immunodetection was performed with the automated Benchmark XT stainer (Ventana, Tucson, AZ) using the Ultraview Universal DAB Detection kit (Ventana). Slides were counterstaining with hematoloxilin II kit (Ventana).

Statistical Analysis

Statistical analysis was performed on GraphPad Prism 5 software (La Jolla, CA) or SPSS v21 (IBM Corp, Armonk, NY). Odds ratios were calculated as previously shown[31]. Two group comparisons were analyzed with two-sided Fisher's exact test. Continuous scale data were calculated with unpaired two-tailed Student's *t* test. *P* values 0.05 were considered

significant. Cox proportional hazards model and significance testing ($\alpha = 0.05$) based on the Wald test were used for multivariate analysis.

Supplementary Material

Refer to Web version on PubMed Central for supplementary material.

Authors

Pawel Buczkowicz[1,2,3,*], Christine Hoeman[4,*], Patricia Rakopoulos[2,3], Sanja Pajovic[2], Louis Letourneau[5], Misko Dzamba[6], Andrew Morrison[2], Peter Lewis[7], Eric Bouffet[8], Ute Bartels[8], Jennifer Zuccaro[2], Sameer Agnihotri[2], Scott Ryall[2], Mark Barszczyk[2,3], Yevgen Chornenkyy[2,3], Mathieu Bourgey[5], Guillaume Bourque[5], Alexandre Montpetit[5], Francisco Cordero[4], Pedro Castelo-Branco[2], Joshua Mangerel[2], Uri Tabori[2,8], King Ching Ho[2], Annie Huang[2,8], Kathryn R. Taylor[9], Alan Mackay[9], Anne E Bendel[10], Javad Nazarian[11], Jason R Fangusaro[12], Matthias A. Karajannis[13], David Zagzag[13], Nicholas K. Foreman[14], Andrew Donson[14], Julia V. Hegert[15], Amy Smith[15], Jennifer Chan[16], Lucy Lafay-Cousin[16], Sandra Dunn[17], Juliette Hukin[17], Chris Dunham[17], Katrin Scheinemann[18], Jean Michaud[19], Shayna Zelcer[20], David Ramsay[20], Jason Cain[21], Cameron Brennan[22], Mark M. Souweidane[22], Chris Jones[9], C. David Allis[7], Michael Brudno[6,23], Oren Becher[4,#], and Cynthia Hawkins[1,2,3,#]

Affiliations

[1]Division of Pathology, The Hospital for Sick Children, The University of Toronto, Canada

[2]The Arthur and Sonia Labatt Brain Tumour Research Centre, The Hospital for Sick Children, Toronto Canada

[3]Department of Laboratory Medicine and Pathobiology, Faculty of Medicine, University of Toronto

[4]Division of Pediatric Hematology/Oncology, Duke University Medical Center, Durham, USA

[5]Genome Quebec Innovation Centre, McGill University, Montreal, Canada

[6]Department of Computer Science, University of Toronto, Canada

[7]Laboratory of Chromatin Biology & Epigenetics, The Rockefeller University, New York, USA

[8]Division of Haematology & Oncology, The Hospital for Sick Children, Toronto, Canada

[9]Division of Cancer Therapeutics, The Institute of Cancer Research, London, United Kingdom

[10]Department of Pediatric Hematology-Oncology, Children's Hospitals and Clinics of Minnesota, Minneapolis, USA

[11]Center for Genetic Medicine, Children's National Medical Center, Washington DC, USA

[12]Department of Pediatrics-Hematology, Ann & Robert H. Lurie Children's Hospital of Chicago, Chicago, USA

[13]Division of Pediatric Hematology/Oncology and Neuropathology, NYU Cancer Institute, NYU Langone Medical Center, New York, USA

[14]Department of Pediatrics, Children's Hospital Colorado, Colorado, USA

[15]Department of Pathology, Arnold Palmer Hospital for Children, Orlando, USA

[16]Clark H. Smith Brain Tumour Centre, Faculty of Medicine, University of Calgary, Calgary, Canada

[17]Department of Pediatric Neurology and Neuro-Oncology, BC Children's Hospital, Vancouver, Canada

[18]Division of Hematology/Oncology, McMaster Children's Hospital, Hamilton, Canada

[19]Department of Pathology and Laboratory Medicine, Children's Hospital of Eastern Ontario, Ottawa, Canada

[20]Department of Hematology/Oncology, Children's Hospital London Health Sciences Centre, London, Canada

[21]Monash Institute of Medical Research, Monash Medical Centre, Clayton, Australia

[22]Department of Neurological Surgery, Weill Cornell Medical College and Memorial Sloan-Kettering Cancer Center, New York, USA

[23]The Centre for Applied Genomics (TCAG), The Hospital for Sick Children, Toronto, Canada

Acknowledgments

References

1. Stiller CA. Population based survival rates for childhood cancer in Britain, 1980–91. BMJ. 1994; 309:1612–6. [PubMed: 7819936]

2. Freeman CR, Perilongo G. Chemotherapy for brain stem gliomas. Childs Nerv Syst. 1999; 15:545–53. [PubMed: 10550585]

3. Maria BL, et al. Brainstem glioma: I. Pathology, clinical features, and therapy. J Child Neurol. 1993; 8:112–28. [PubMed: 8505473]

4. Hargrave D, Bartels U, Bouffet E. Diffuse brainstem glioma in children: critical review of clinical trials. Lancet Oncol. 2006; 7:241–8. [PubMed: 16510333]

5. Donaldson SS, Laningham F, Fisher PG. Advances toward an understanding of brainstem gliomas. J Clin Oncol. 2006; 24:1266–72. [PubMed: 16525181]

6. Buczkowicz P, et al. Aurora Kinase B Is a Potential Therapeutic Target in Pediatric Diffuse Intrinsic Pontine Glioma. Brain Pathol. 2012

7. Paugh BS, et al. Genome-wide analyses identify recurrent amplifications of receptor tyrosine kinases and cell-cycle regulatory genes in diffuse intrinsic pontine glioma. J Clin Oncol. 2011; 29:3999–4006. [PubMed: 21931021]

8. Paugh BS, et al. Integrated molecular genetic profiling of pediatric high-grade gliomas reveals key differences with the adult disease. J Clin Oncol. 2010; 28:3061–8. [PubMed: 20479398]

9. Zarghooni M, et al. Whole-genome profiling of pediatric diffuse intrinsic pontine gliomas highlights platelet-derived growth factor receptor alpha and poly (ADP-ribose) polymerase as potential therapeutic targets. J Clin Oncol. 2010; 28:1337–44. [PubMed: 20142589]

10. Khuong-Quang DA, et al. K27M mutation in histone H3.3 defines clinically and biologically distinct subgroups of pediatric diffuse intrinsic pontine gliomas. Acta Neuropathol. 2012; 124:439–47. [PubMed: 22661320]

11. Schwartzentruber J, et al. Driver mutations in histone H3.3 and chromatin remodelling genes in paediatric glioblastoma. Nature. 2012; 482:226–31. [PubMed: 22286061]

12. Wu G, et al. Somatic histone H3 alterations in pediatric diffuse intrinsic pontine gliomas and non-brainstem glioblastomas. Nat Genet. 2012; 44:251–3. [PubMed: 22286216]

13. Herbert BS, Shay JW, Wright WE. Analysis of telomeres and telomerase. Curr Protoc Cell Biol. 2003; Chapter 18(Unit 18):6.

14. Henson JD, et al. DNA C-circles are specific and quantifiable markers of alternative-lengthening-of-telomeres activity. Nat Biotechnol. 2009; 27:1181–5. [PubMed: 19935656]

15. Kowanetz M, Valcourt U, Bergstrom R, Heldin CH, Moustakas A. Id2 and Id3 define the potency of cell proliferation and differentiation responses to transforming growth factor beta and bone morphogenetic protein. Mol Cell Biol. 2004; 24:4241–54. [PubMed: 15121845]

16. Kurooka H, Nakahiro T, Mori K, Sano K, Yokota Y. BMP signaling is responsible for serum-induced Id2 expression. Biochem Biophys Res Commun. 2012; 420:281–7. [PubMed: 22421219]

17. Shin M, et al. Identification of a novel bone morphogenetic protein (BMP)-inducible transcript, BMP-inducible transcript-1, by utilizing the conserved BMP-responsive elements in the Id genes. J Bone Miner Metab. 2013; 31:34–43. [PubMed: 22976053]

18. Song GA, et al. Molecular consequences of the ACVR1(R206H) mutation of fibrodysplasia ossificans progressiva. J Biol Chem. 2010; 285:22542–53. [PubMed: 20463014]

19. Kaplan FS, et al. Classic and atypical fibrodysplasia ossificans progressiva (FOP) phenotypes are caused by mutations in the bone morphogenetic protein (BMP) type I receptor ACVR1. Hum Mutat. 2009; 30:379–90. [PubMed: 19085907]

20. Petrie KA, et al. Novel mutations in ACVR1 result in atypical features in two fibrodysplasia ossificans progressiva patients. PLoS One. 2009; 4:e5005. [PubMed: 19330033]

21. Chen XS, Zhang YH, Cai QY, Yao ZX. ID2: A negative transcription factor regulating oligodendroglia differentiation. J Neurosci Res. 2012; 90:925–32. [PubMed: 22253220]

22. Liu Z, et al. Overexpressed DNA-binding protein inhibitor 2 as an unfavorable prognosis factor promotes cell proliferation in nasopharyngeal carcinoma. Acta Biochim Biophys Sin (Shanghai). 2012; 44:503–12. [PubMed: 22551584]

23. Rollin J, et al. The intracellular localization of ID2 expression has a predictive value in non small cell lung cancer. PLoS One. 2009; 4:e4158. [PubMed: 19129913]

24. Wazir U, Jiang WG, Sharma AK, Newbold RF, Mokbel K. The mRNA expression of inhibitors of DNA binding-1 and -2 is associated with advanced tumour stage and adverse clinical outcome in human breast cancer. Anticancer Res. 2013; 33:2179–83. [PubMed: 23645773]

25. Li H, Durbin R. Fast and accurate long-read alignment with Burrows-Wheeler transform. Bioinformatics. 2010; 26:589–95. [PubMed: 20080505]

26. Jiang Y, Wang Y, Brudno M. PRISM: pair-read informed split-read mapping for base-pair level detection of insertion, deletion and structural variants. Bioinformatics. 2012; 28:2576–83. [PubMed: 22851530]

27. Mills RE, et al. Natural genetic variation caused by small insertions and deletions in the human genome. Genome Res. 2011; 21:830–9. [PubMed: 21460062]

28. Fiume M, et al. Savant Genome Browser 2: visualization and analysis for population-scale genomics. Nucleic Acids Res. 2012; 40:W615–21. [PubMed: 22638571]

29. Medvedev P, Fiume M, Dzamba M, Smith T, Brudno M. Detecting copy number variation with mated short reads. Genome Res. 2010; 20:1613–22. [PubMed: 20805290]

30. Sasai K, et al. O6-methylguanine-DNA methyltransferase is downregulated in transformed astrocyte cells: implications for anti-glioma therapies. Mol Cancer. 2007; 6:36. [PubMed: 17547775]

31. Bland JM, Altman DG. Statistics notes. The odds ratio. BMJ. 2000; 320:1468. [PubMed: 10827061]

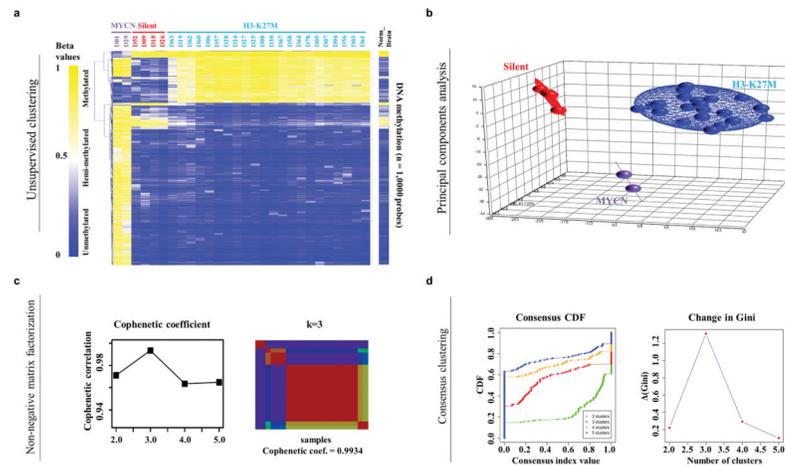**Figure 1. Methylation profiling reveals three molecular subgroups of DIPG**

(**a**) Heat map of methylation levels in three DIPG subgroups identified by unsupervised hierarchical clustering and supported by (**b**) principal components analysis, (**c**), non-negative matrix factorization (cophenetic coefficient = 0.9934, k=3) and (**d**) consensus clustering represented by cumulative distribution function and change in Gini.

Figure 2. Molecular subgroups of DIPG share common clinical features and recurrent genomic events

(**a**) Clinical and genomic features such as gender, histology, frequency of recurrent mutations, alternative lengthening of telomeres and copy number alterations are represented in a DIPG subgroup specific manner. (**b**) Probability of two mutational or structural features of DIPG co-occurring based on odds ratio suggests statistically significant association between K27M-H3.3 and *PDGFRA* amplifications (OR = 8.0, p = 0.0127) and between K27M-H3.1 and *ACVR1* mutations (OR = 15.8, p < 0.001). (**C**) Probability of mutations or structural event of DIPG occurring with a clinical feature such as gender or tumor histology based on odds ratio shows statistically significant correlation between *P53* mutations and GBM histology (OR = 10.8, p < 0.005), among others.
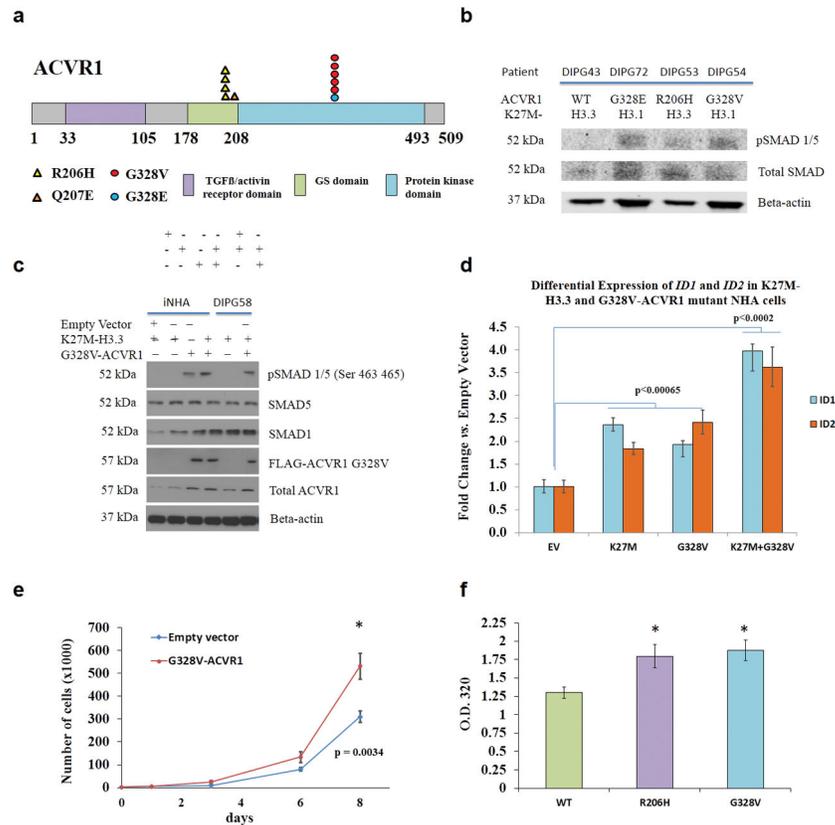
Figure 3. *ACVR1* mutations constitutively activate BMP signaling *in vitro* and in *ACVR1* mutant DIPG

(**a**) Four mutations (R206H, Q207E, G328E and G328V) were detected in 12/61 DIPG patients. The R206H and Q207E mutations occur in the GS domain and the G328-mutations occur in the protein kinase domain. (**b**) Human DIPG with *ACVR1* mutations have increased pSMAD1/5 expression compared with *ACVR1* wild-type DIPG. (**c**) Western blot showing increased pSMAD1/5 in *ACVR1* mutant NHA and DIPG58 cells transfected with G328V-ACVR1 as compared to control cells. (**d**) Real-time PCR in NHA transfected with empty vector, K27M-H3.3, G328V-ACVR1 or a combination of K27M-H3.3 and G328V-ACVR1 shows increase in *ID1* and *ID2* gene expression as compared to empty vector control. Error bars represent standard deviation. (**e**) Mutant G328V-ACVR1 expressing NHA cells have an increased growth rate as compared to empty vector controls (p = 0.0034). (**f**) Compared to WT-ACVR1 murine brainstem progenitor cultures, mutant *ACVR1* has significantly higher BrdU incorporation suggesting increased proliferation (* p<0.05). Error bars represent standard error of the mean.

Table 1

Clinical, genetic and epigenetic features of diffuse intrinsic pontine glioma molecular subgroups.

	MYCN	Silent	H3-K27M
Gender			
Male:Female	1:3	2:1	1:1
Histology			
Gr. II	0%	33%	0%
Gr. III	0%	11%	26%
Gr. IV	100%	56%	74%
Mutations			
K27M-H3.3	0%	35%	97%
ACVR1	0%	22%	18%
CpG Methylation			
Med. Beta value	0.75	0.13	0.15
Copy Number Alterations			
	MYCN amplification, Chr. 2p chromothripsis	Few copy number changes, silent genomes	PVT1-/MYC& PDGFRA gains/amp, RB1 &TP53 deletions
ALT phenotype			
ALT +	0%	0%	22%
Gene Expression Profiling			
	overexpression of DYX2, HSPR12, FAP	overexpression of MDM2, MSMP, ADAM33	underexpression of VAX2, HOXC6, HOXA9, HOXA7, DOXD4
Age of diagnosis			
Med. Age of Diagnosis	6.3 yrs	5 yrs	7 yrs